Transonic Shock-Wave/Turbulent Boundary-Layer Interactions in a Circular Duct

Deepak Om*
University of Washington, Seattle, Washington
John R. Viegas†
NASA Ames Research Center, Moffett Field, California
and
Morris E. Childs‡
University of Washington, Seattle, Washington

Detailed pitot, static, and wall pressure measurements have been obtained for a transonic normal shock-wave/turbulent boundary-layer interaction at freestream Mach numbers of 1.28, 1.37, and 1.48, and at a constant unit Reynolds number of 4.92×10^6/m in an axisymmetric, internal flow. Measurements have also been obtained at a unit Reynolds number of 9.84×10^6/m at a freestream Mach number of 1.29. The interaction depends very strongly on the Mach number. The effect of Reynolds number on the unseparated interaction is small. Flow blockage due to the wind tunnel wall boundary layer produces a weaker interaction and a much larger supersonic tongue than observed for planar flows. Comparisons are made with solutions to the time-dependent, mass-averaged, Navier-Stokes equations incorporating a two-equation, Wilcox-Rubesin turbulence model. The computations are in agreement with the experimental results.

Nomenclature

B = blockage, $1-(1-\delta_u^*/R)^2$
c_f = skin-friction coefficient, $2\tau_w/\rho_e u_e^2$
M = Mach number
P = pressure
R = radius of test section
Re = Reynolds number
T = temperature
u = streamwise velocity
x = axial distance
$\bar{X}$ = $(x-x_u)/\delta_u$
y = radial distance from the wall
$\bar{Y}$ = y/δ_u
δ = boundary-layer thickness
δ^* = displacement thickness, given by

$$\delta^*-\frac{\delta^{*2}}{2R}=\int_0^\delta\left(1-\frac{\rho u}{\rho_e u_e}\right)\left(1-\frac{y}{R}\right)\mathrm{d}y$$

θ = momentum thickness, given by

$$\theta-\frac{\theta^2}{2R}=\int_0^\delta\frac{\rho u}{\rho_e u_e}\left(1-\frac{u}{u_e}\right)\left(1-\frac{y}{R}\right)\mathrm{d}y$$

ρ = density
τ = total shear stress

Subscripts

e = boundary-layer edge
t = pitot
u = start of interaction
w = wall value
0 = stagnation condition
∞ = freestream condition at start of interaction

Introduction

TRANSONIC normal shock-wave/turbulent boundary-layer interactions represent an important problem in fluid mechanics because of the occurrence of such interactions in both external and internal aerodynamic flows. Important examples are those occurring on wings in transonic flight (external) and in the inlet of air breathing engines (internal). In internal interactions, the flow blockage due to the wall boundary layers may produce a flowfield different from that occurring in external flows.[1,2] Detailed flowfield measurements in internal flow interactions are needed to understand the effects of blockage. Also, measurements are needed for the evaluation of computational methods for such flows. Computational schemes employing the Navier-Stokes equations are attractive because they simultaneously compute the viscous and inviscid flowfields. An important factor in the success of Navier-Stokes computations is the use of adequate turbulence models. Experimental data obtained in interactions such as the one investigated in this study are needed to evaluate various turbulence models.

Several investigations of the mean flow properties of normal shock-wave/turbulent boundary-layer interaction at transonic speed have been conducted.[1-8] These flows were either planar two-dimensional[2,3,5,6] or axially symmetric two-dimensional.[1,4,7,8] Three-dimensional effects are known to be present in shock/boundary-layer interaction studies performed in planar two-dimensional facilities.[6,9,10] The purpose of the present study was to investigate experimentally the effects of Mach number, Reynolds number, and flow blockage on a normal shock-wave/turbulent boundary-layer interaction and to evaluate a Navier-Stokes analysis for computing such interactions. Detailed mean flow measurements were obtained

Presented as Paper 82-0990 at the AIAA/ASME Third Joint Thermophysics, Fluids, Plasma and Heat Transfer Conference, St. Louis, Mo., July 7-11, 1982; received Oct. 5, 1983; revision received May 14, 1984.

*Research Assistant Professor, Department of Mechanical Engineering. Currently with Boeing Commercial Airplane Company, Seattle, Wash. Member AIAA.

†Research Scientist, Experimental Fluid Dynamics Branch. Member AIAA.

‡Professor, Department of Mechanical Engineering. Member AIAA.

at various Mach and Reynolds numbers in an axisymmetric internal duct with minimal three-dimensional effects. Numerical computations were performed in which the Navier-Stokes equations with a two-equation Wilcox-Rubesin model of the turbulence were solved to predict this complex flow. This turbulence model was selected for these calculations because of the relative success when using it, in comparison with other turbulence models, to simulate a variety of complex turbulent flows containing shock-wave/boundary-layer interactions.[1] Only the in-flow conditions, the approximate shock location, and the downstream pressure were provided to the computor (Viegas). Based on these conditions, the numerical simulation was completed. This paper compares these predicted numerical results with the measured experimental results.

Experiment

The experiment was performed in the continuous-flow facility[11] at the University of Washington. The facility is shown schematically in Fig. 1. Three axisymmetric nozzles with nominal Mach numbers of 1.5, 1.4, and 1.3 were used in conjunction with a constant 5.19-cm-diam test section. The contours of the nozzles were not corrected for boundary-layer growth. The overall length of the plexiglas nozzle-test-section facility was 24.13 cm. Static pressure taps were located on a line in the constant diameter test section at varying intervals of 2.54, 5.08, and 6.35 mm. Additional taps were located at 90-deg intervals around the test section from this primary line in order to check flow symmetry. Boundary-layer trips were cemented to the converging part of the nozzle to make sure the test section boundary layer was turbulent. The normal shock wave was generated at the desired location in the test section using a blunt cone as a centerbody to choke the flow at the exit from the test section.

A 55.88 mm long by 5.08 mm wide slot cut through the wall was provided near the diffuser end, allowing for the radial and longitudinal translation of probes. Pitot and static pressure probes with distances from the stem centerline to the measuring location of 101, 152, and 197 mm were used to obtain pressure distributions. Measurements with longer probes were checked against measurements with a shorter probe to make sure that there was no deflection of the probe tip due to dynamic pressure in the operating total pressure range. For measurements in the flow facility with nozzles of nominal Mach numbers of 1.5 and 1.4, a probe 197 mm long was used. The probe could be translated over the complete length of measuring locations with the addition of small extension sections of constant diameter between the test section and the diffuser. The flow in the test section was not affected by the addition of the extension sections. On the other hand, with the nozzle of nominal Mach number of 1.3, the addition of extension sections choked the flow producing a shock which could not be positioned at the desired location. Thus, for the lowest Mach number, three probes of different lengths were used. Probes were inserted into the test section from the diffuser end to minimize blockage of the flow. During the experiment, small changes in probe blockage due to traversing of the probe were offset by moving the centerbody and ensuring that the normal shock remained in a fixed position in the test section. The wall pressure distribution was used to monitor the shock location.

Pitot pressures were measured with a flattened pitot tube[11] for which the probe tip was approximately 0.254 mm high and the opening was approximately 0.1 mm high by 0.38 mm wide. Local static pressures were measured with a cone-cylinder probe of the type described in Ref. 12. The outside diameter of the probe was 1.06 mm. Two 0.16-mm-diam static pressure ports, located 10.6 mm downstream of the cone-cylinder junction, were drilled at ± 40 deg circumferentially from the side of the probe that was closest to the test section wall. Static pressure ports at these locations make the probe relatively insensitive to flow inclination in the range of -2 to $+6$ deg. Probes and instrumentation are described in detail in Ref. 13.

Following Ref. 14, the experimental uncertainty of the measured pressures was estimated as $\pm(F+\sigma t_{95})$, where F is the fixed error, σ the standard deviation of a set of repeated measurements, and t_{95} the 95th percentile of the student-t distribution. The uncertainty for wall pressure was $\pm 0.5\%$, for pitot pressure $\pm 1.0\%$, and for static pressure $\pm 5.0\%$.

The test facility was operated with dry air at a nominal stagnation temperature of 300 K ($\pm 1\%$). For flows at freestream Mach numbers of 1.48, 1.37, and 1.28, the Reynolds number based on freestream static temperature was 4.92×10^6/m. For flow at the freestream Mach number of 1.29, the Reynolds number was 9.84×10^6/m. The range of Reynolds number was limited by the suction capacity of the flow facility.

Numerical Simulation

The computational procedures used are essentially those described in detail in Ref. 15. The differential equations used to describe the mean flow for this study are the time-dependent, mass-averaged, Navier-Stokes equations for axially symmetric flow of a compressible fluid. These equations are augmented by two additional equations for the field variables (kinetic energy and dissipation rate) associated with the Wilcox-Rubesin model of turbulence.[16] Restrictions on the differential equations include the perfect gas assumption, constant specific heats, the Sutherland viscosity law, and zero bulk viscosity. The two-equation Wilcox-Rubesin model of turbulence was selected for this study based on experiences with it and other turbulence models for a variety of complex flows. In studies presented in Refs. 8 and 15 and at the recent AFOSR/Stanford Conference on Complex Flows,[17] the Wilcox-Rubesin model was shown to be effective for modeling the turbulence for this type of flow. The modeling coefficients used with this turbulence model are those described in Ref. 15.

The numerical algorithm used here is the basic explicit second-order, predictor-corrector, finite-difference, time-splitting method of MacCormack[18] modified by the efficient explicit-implicit-characteristic algorithm of Ref. 19. A description of this method, along with its adaptation to the Wilcox-Rubesin turbulence model equations, is contained in Refs. 15 and 20. The computational domain consists of a control volume that includes the interaction and extends from the wall to the centerline of the test section. This domain is divided into a two-mesh system. An exponentially stretched fine mesh is used near the wall where the viscous effects are important. The outer flow, which is predominantly inviscid, is described using a uniform coarse mesh. A uniform mesh, containing about four mesh points per δ_u, is used in the flow direction.

For all Mach numbers the upstream boundary of the control volume was about $3\delta_u$ ahead of the initial rise in surface pressure. A total of 128 mesh points were used in the streamwise direction for the two lower Mach number cases, while 170 mesh points were used for the higher Mach number cases. Normal to the surface 40 mesh points were used. Typically, about 30 of these points were in the boundary layer. Transfer from the exponentially stretched fine mesh to the coarse mesh occurs near the outer edge of the boundary layer. The distance of the first mesh point from the wall was selected small enough that the solutions are independent of this spacing (typically within $y^+_{\min}\equiv y\sqrt{\tau_w\rho_w/\mu_w}\lesssim 0.2$ where μ is the molecular viscosity). The large number of mesh points used for these

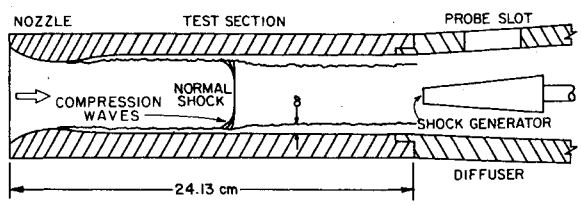

Fig. 1 Experimental facility.

calculations resulted in computing times that varied from 3.5 to 5 h to obtain fully converged solutions on a CDC 7600.

For the simulations presented here, the inviscid flow at the upstream boundary of the control volume was uniform, steady, and supersonic at the experimental freestream Mach number. The properties in the upstream boundary layer were obtained from the nonsimilar boundary-layer code of Ref. 16. This code provided detailed profiles as a function of streamwise location. These profiles were self-consistent with the mean flow parameters, but none of them agrees with every aspect of the experimental profile at the beginning of the pressure rise. The selected starting profile was one that had a momentum thickness that closely matched the experimental value at the beginning of the pressure rise. The momentum thickness was matched because it can be determined with reasonable certainty. This choice also results in fair agreement of the other boundary-layer parameters, such as δ_u^*, θ_u, and C_{f_u}, with those of the experiment at the in-flow boundary. At the downstream boundary, the experimental value of the static pressure was used, and a special technique[1] was used to inhibit the upstream propagation of disturbances from this boundary. A more complete description of the boundary conditions, along with special procedures used for the turbulence model variables and equations, is contained in Refs. 15 and 21.

Results and Discussion

The experimental results are presented in conjunction with the results of the numerical predictions for varying Mach numbers and Reynolds numbers. The study of the effect of Reynolds number was limited to the lowest Mach number. A summary of the experimental test conditions and upstream boundary-layer parameters is given in Table 1. The effect of blockage can be measured by the parameter B $[=1-(1-\delta_u^*/R)^2]$ which is defined as the effective area reduction due to boundary-layer growth at the upstream location, divided by the test section area.

In the comparisons of the experimental results with those of the numerical predictions, it should be noted that the normalization factors for the experiment are determined from the experimental measurements while those for the numerical results are determined from the numerical solutions. Since no attempt was made to precisely match upstream numerical parameters with experimental ones, some of the factors used in normalizing the numerical results differ slightly from those given in Table 1. Table 2 contains the upstream boundary-layer parameters used in normalizing the numerical results. The difference between the upstream boundary-layer parameters of Table 2 and those of Table 1 result from the choice of the in-flow boundary conditions of the numerical control volume as discussed in the previous section. Normalizing the results in the manner discussed above provides a consistent comparison of calculation with experiment between the point of the initial pressure rise and the downstream boundary, independent of the details of comparison ahead of the interaction. When the numerical calculations are normalized by the values from Table 1 rather than those from Table 2 the results are not altered significantly and the comparisons with experiment will remain as discussed in the following sections.

The upstream boundary-layer profiles for the three test cases are shown in semilogarithmic form in Fig. 2. Also shown for comparison are the compressible wall-wake profiles,[22] with which the data points are in good agreement. For all of the test cases, the skin friction at the upstream location ($\bar{X}=0$) is within 5% of the zero pressure gradient flat-plate value as determined from Ref. 23. It was found that, for every test case, the upstream boundary layer was typical of a turbulent equilibrium boundary-layer profile.

Wall Pressure

In Fig. 3, the wall pressure is normalized by the value just upstream of the initial pressure rise. The distance $\bar{X}$ is measured from the point of the initial pressure rise and is normalized by the boundary-layer thickness δ_u at the start of the pressure rise. The steepest slope in the wall pressure is observed near the start of the interaction, with the slope increasing with increasing Mach number and also with increasing Reynolds number. The overall pressure recovery is lower than the Rankine-Hugoniot value because with the thickening of

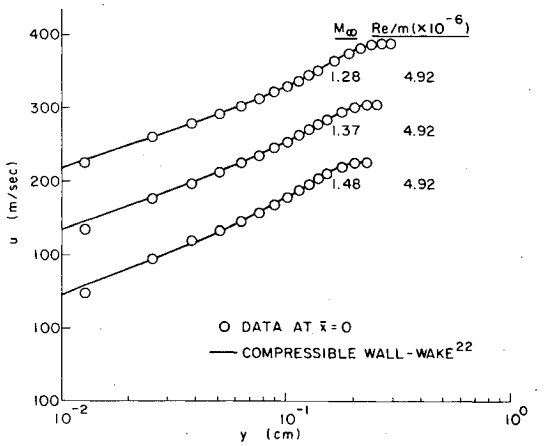

Fig. 2 Comparison of upstream experimental boundary-layer velocity profiles with compressible wall-wake profiles.

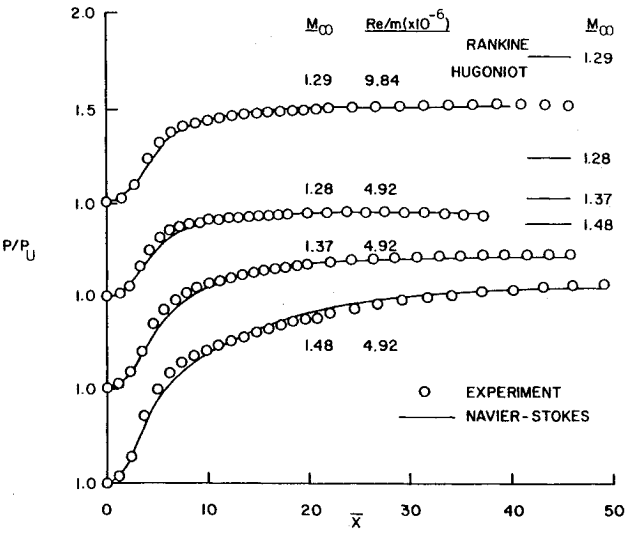

Fig. 3 Wall pressure distribution.

Table 1 Experimental flow conditions and upstream boundary-layer parameters

P_0, atm	M_∞	Re/m, $\times 10^{-6}$	δ_u, mm	δ_u^*, mm	θ_u, mm	C_{f_u}	B
0.3325	1.48	4.92	2.10	0.438	0.181	0.003725	0.0227
0.3264	1.37	4.92	2.34	0.455	0.199	0.003647	0.0236
0.3239	1.28	4.92	2.62	0.509	0.229	0.003734	0.0264
0.6477	1.29	9.84	2.13	0.408	0.187	0.003177	0.0212

Table 2 Computational flow conditions and upstream boundary-layer parameters

P_0, atm	M_∞	Re/m, $\times 10^{-6}$	δ_u, mm	δ_u^*, mm	θ_u, mm	C_{f_u}	B
0.3325	1.48	4.92	2.03	0.495	0.194	0.003247	0.0256
0.3264	1.37	4.92	2.14	0.491	0.204	0.003305	0.0254
0.3239	1.28	4.92	2.05	0.474	0.210	0.003229	0.0246
0.6477	1.29	9.84	1.87	0.400	0.181	0.002986	0.0208

the boundary layer through the shock wave, the effective downstream area is reduced which produces a lower pressure. The computations capture the Reynolds number and Mach number effects and quantitative pressure levels very well throughout the interaction region (Fig. 3).

Static Pressure

Figure 4 shows a comparison of experimental and numerically determined flowfield static pressure profiles at a few axial locations in the vicinity of the shock wave for the freestream Mach number of 1.48. In the region before the shock wave and outside the boundary layer, the static pressure has also been determined using pitot pressure and the tunnel stagnation pressure P_0 as the local total pressure, since losses through the compression waves emanating from the wall boundary layer are small.

In the region ahead of the shock wave and outside the boundary layer, the static pressure determined from pitot pressure agrees well with the Navier-Stokes numerical computation but differs from the measured static pressure (Fig. 4). The precise reasons for the difference are not clear. However, one factor may be that the interaction of the normal shock wave and/or emanating compression waves from the wall boundary layer with the boundary layer on the static probe affected the static pressure readings. In this region the pitot pressure and the plenum pressure were used to determine the Mach number.

At $\bar{X}=2.42$, the measured static pressure shows large interference effects near the wall. This interference probably is caused by the upstream influence of the interaction of the emanating compression waves from the wall boundary layer with the boundary layer on the static probe. Since the measured static pressure near the wall is inaccurate, a linear distribution between the measured wall pressure and the measured static pressure at $\bar{Y}=0.5$ was used in determining Mach number.

Just after the shock wave, the measured static pressure increases as $\bar{Y}$ increases. It becomes nearly constant and equal to the wall pressure at $\bar{X}=12.10$ and at locations farther downstream. The numerical computation describes these experimental observations very well. The overall pattern of variation of static pressure observed for the three other test cases is similar.[13]

Mach Number Contours

Figure 5 shows experimental and computed Mach number contours for the flowfield at a freestream Mach number of 1.48. The experimental contours were determined from measured pitot and static pressures except in the region ahead of the shock wave and ouside the boundary layer as discussed in the previous section. Since it was not possible to obtain schlieren or shadowgraph pictures of the flow in the circular duct, the exact structure and location of the shock could not be determined. The approximate experimental shock location, as determined from static pressure profiles, is indicated in Fig. 5a. The location of the vortex layer was found from the pitot pressure profiles. The flow remains supersonic as it passes through the system of compression waves emanating from the boundary layer at the foot of the shock wave and produces a large supersonic region embedded in an otherwise subsonic flow. This region has been termed the "supersonic tongue" by Seddon[2] ($M_\infty=1.47$), Kooi[6] ($M_\infty=1.44$), and East[7]

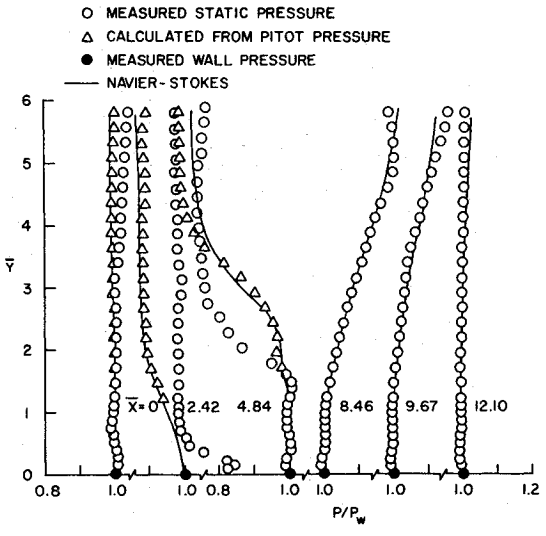

Fig. 4 Static pressure profiles: $M_\infty=1.48$, $Re/\text{m}=4.92\times10^6$.

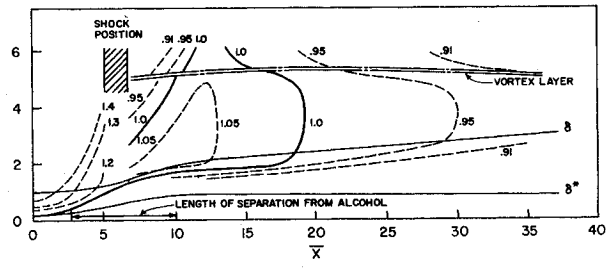

Fig. 5a Experimental Mach number contours: $M_\infty=1.48$, $Re/\text{m}=4.92\times10^6$.

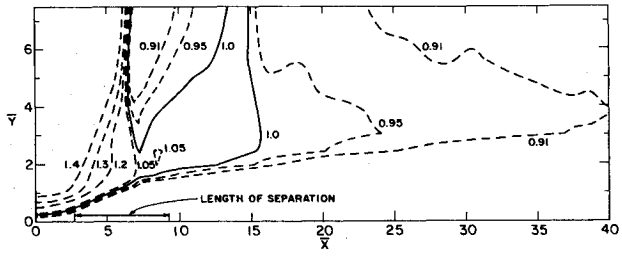

Fig. 5b Computed Mach number contours: $M_\infty=1.48$, $Re/\text{m}=4.92\times10^6$.

($M_\infty=1.40$). The embedded supersonic region does not look like the tongue reported by Seddon.[2] Instead, its height increases with distance downstream from the shock wave. This large region of the embedded supersonic flow is due to an increased flow blockage in the test section. Thickening of the boundary layer through the shock wave reduces the effective downstream area, producing a lower pressure and, hence, increasing the streamwise extent of the embedded supersonic flow. An increase in the radial extent of the embedded supersonic flow is associated with the buildup of displacement thickness. In Ref. 24, with an increase in upstream displace-

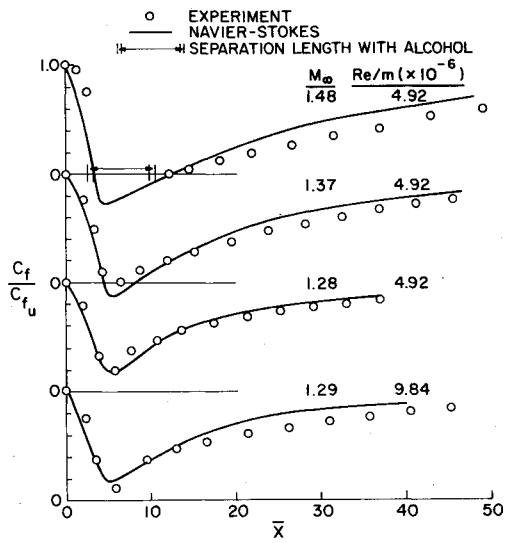

Fig. 6 Skin-friction distribution.

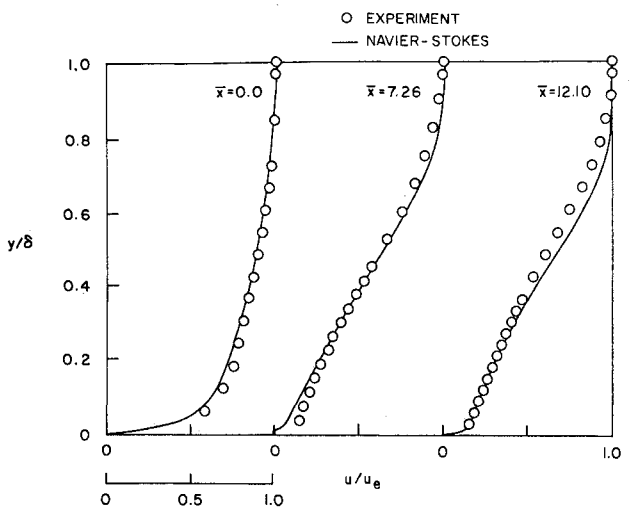

Fig. 7a Boundary-layer velocity profiles: $M_\infty = 1.48$, $Re/m = 4.92 \times 10^6$.

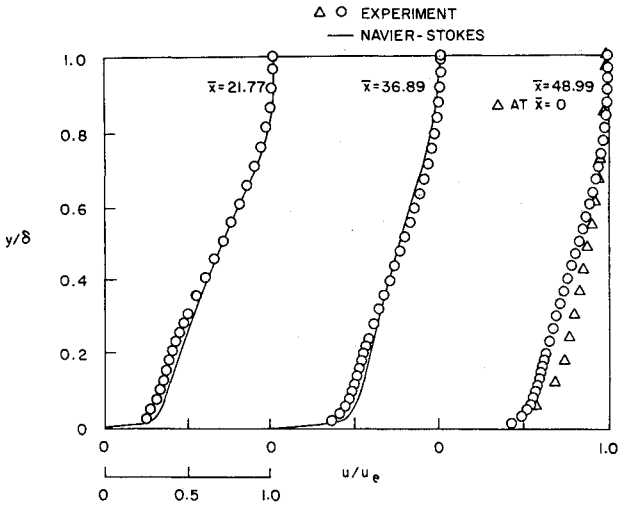

Fig. 7b Boundary-layer velocity profiles: $M_\infty = 1.48$, $Re/m = 4.92 \times 10^6$.

ment thickness (and hence blockage) at nearly the same freestream Mach number and unit Reynolds number, the displacement buildup chokes the flow producing a large embedded supersonic region that completely fills the duct and is terminated by another shock wave.

The computed Mach number contours of Fig. 5b indeed capture the qualitative structure shown in Fig. 5a including the shock location and the shape of the embedded supersonic region. However, the computed embedded supersonic region behind the shock is somewhat smaller than the experimental measurements indicate. The wiggles in the computed Mach contours that occur when the slope $(\partial \bar{Y}/\partial \bar{X})_M$ is relatively small and the absence of the vortex layer are due to the coarseness of the mesh in the radial direction outside the boundary layer. Comparison of the experimental and computed Mach number contours for the three other test cases can be found in Ref. 13. The size of the embedded supersonic region decreases with decreasing Mach number and increasing Reynolds number. The computed embedded supersonic region is somewhat smaller than the experimental measurements indicate for all three test cases.

Skin Friction

The symbols in Fig. 6 represent skin friction determined from the experimental mean velocity profiles using the law-of-the-wall fit of Rubesin et al.[25] Details regarding the determination of the skin friction can be found in Ref. 21. An alcohol technique[11] was used to find the region of separated flow. For $M_\infty = 1.48$, the alcohol technique indicates separation as shown in Fig. 6. Velocity profiles were not used to determine skin friction in the separated region observed by alcohol because of the uncertainty of the experimental data near the separated region. No attempt was made to extrapolate experimental skin friction to find the separation point because of insufficient data just ahead of separation. At $M_\infty = 1.37$, separation could not be detected with alcohol although an extrapolation of experimental skin friction would indicate a small region of separation. The boundary layer at the lower Mach numbers is unseparated. It can be seen that the effect of Mach number on skin friction is very pronounced. The effect of Reynolds number is small on the unseparated interaction.

Downstream of the shock wave, the skin friction increases gradually for all of the test cases. For $M_\infty = 1.48$, the skin friction at $\bar{X} = 49.88$ is still 27.5% lower than the zero pressure gradient flat-plate value[23] at the corresponding Mach and Reynolds numbers, indicating that the boundary layer still has not recovered from the effects of the interaction. For $M_\infty = 1.28$, on the other hand, the skin friction at $\bar{X} = 36.84$ is only 3.5% lower than the zero pressure gradient flat-plate value[23] at the corresponding Mach and Reynolds numbers.

The skin friction from the Navier-Stokes simulation, as shown in Fig. 6, is somewhat different from that reported earlier in Ref. 21. In the present paper, skin friction was determined from the computed velocity profiles using the method of Rubesin et al.[25] to maintain consistency with the determination of skin friction from experimental data. At lower Mach numbers where the flow is unseparated and near separation, the numerical predictions of skin friction agree very well with values determined from experimental data. At the highest Mach number of 1.48 where the flow is separated, the agreement is not as good.

A comparison of separation length from the present investigation with the available planar two-dimensional experimental results (summarized in Refs. 6, 13, and 26) suggests that the effect of the flow blockage is to reduce the extent of separation. This is in agreement with the results of Mateer and Viegas.[1] In Ref. 1 it was shown that flow blockage prevented axisymmetric transonic shock-wave/turbulent boundary-layer flows from separating relative to similar but two-dimensional flows on flat plates. Thus, flow blockage has an effect of producing a weaker interaction.

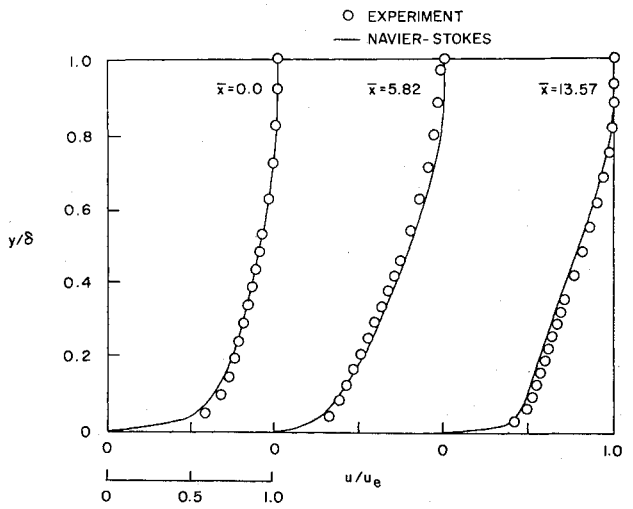

Fig. 8a Boundary-layer velocity profiles: $M_\infty = 1.28$, $Re/m = 4.92 \times 10^6$.

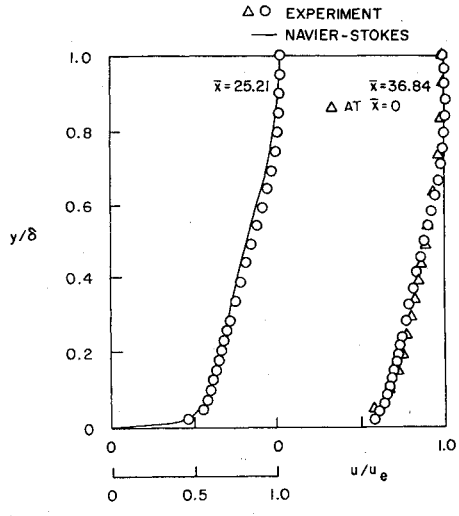

Fig. 8b Boundary-layer velocity profiles: $M_\infty = 1.28$, $Re/m = 4.92 \times 10^6$.

Boundary-Layer Velocity Profiles

Boundary-layer velocity profiles upstream of, within, and downstream of the interaction region for $M_\infty = 1.48$ and 1.28 are shown in Figs. 7 and 8. The experimental velocity profiles were determined from measured pitot and static pressures, using the assumption that the total temperature across the boundary layer was constant. A least-squares wall-wake fit[22] to the experimental data was used to obtain the boundary-layer thickness. Mathews et al.[27] earlier demonstrated the use of this technique for flows with normal shock waves. Although the alcohol technique clearly indicated separation for $M_\infty = 1.48$, an area of reversed flow cannot be distinguished from the experimental velocity profiles. Values of velocity deduced from measured pitot pressures near the separated region tend to be too high. Similar results were obtained by Vidal et al.[5] and Kooi.[6] For the freestream Mach number of 1.48 (Fig. 7), a comparison of the boundary-layer velocity profile at $\bar{X} = 48.99$, with the undisturbed velocity profile at $\bar{X} = 0$, indicates that the velocity profile has not fully recovered to the undisturbed state. There is a noticeable velocity defect in the range $0.1 < y/\delta < 0.6$, indicating a strong wake component not yet relaxed from the effects of the interaction. For the lowest freestream Mach number of 1.28, the boundary layer appears to have returned to essentially the undisturbed state at $\bar{X} = 36.84$, as is shown in Fig. 8.

The numerically determined velocity profiles presented in Figs. 7 and 8 show overall good agreement with the experimental velocity profiles where the boundary-layer thickness for the numerically predicted velocity profiles was determined as explained in the next subsection entitled "Displacement and Momentum Thicknesses." This agreement is especially good for the lowest Mach number case, Fig. 8. At the highest Mach number, the computation and experiment agree at the start of the interaction, but disagree very close to the wall in the reattachment and recovery regions. Also, they disagree over a larger distance from the wall in the computed separation regions. These differences could be due to weaknesses in the turbulence model in the separation and downstream of the reattachment region. These weaknesses have been noted in the past[15] as a definite characteristic of the Wilcox-Rubesin turbulence model used in the present study. The differences near the separated region could also be due to the inaccuracies in the measurements for reasons discussed earlier. These differences between the experimentally and numerically determined velocity profiles near the wall are reflected in the skin-friction comparisons in Fig. 6.

Displacement and Momentum Thicknesses

The upstream experimental displacement and momentum thicknesses were obtained by a least-squares wall-wake fit[22] to the experimental data. The displacement thickness increases rapidly at the start of the interaction, reaches a maximum value, and then decreases gradually, as shown in Fig. 9. The maximum buildup is a strong function of the freestream Mach number, increasing with increasing Mach number. Seddon[2] found a maximum increase of the displacement thickness of 5.6 times the undisturbed value at a freestream Mach number of 1.47. In the present experiment, for a freestream Mach number of 1.48, the increase is 4.2 times the undisturbed value. Although Re_{δ_u} is somewhat higher for Seddon's experiment,[2] the difference between the results of Seddon and the present study probably is due to the higher blockage in the present experiment. This conclusion is further substantiated by the results of Ref. 24 where an increased blockage, as compared with the present experiment, reduces the ratio of displacement thickness buildup, although the value of maximum displacement thickness becomes higher. The effect of the Reynolds number on the displacement thickness buildup is small for the unseparated interaction. Momentum thickness continuously increases downstream, as is shown in Fig. 10. With increasing Mach number, larger increases in momentum thickness occur. The Reynolds number effect on the momentum thickness is small for the unseparated interaction.

The intergral thicknesses from the Navier-Stokes solution, as shown in Figs. 9 and 10, were calculated as follows: Before the shock wave, where static pressure decreases as $\bar{Y}$ increases, the upper limit on the integration to determine δ^* and θ is based on 0.995 of $(\rho u)_{\max}$ (i.e., integrate normal to the wall to y where ρu is 0.995 of the maximum). After the shock wave where the static pressure increases as $\bar{Y}$ increases, the upper limit on the integration to determine δ^* and θ is based on 0.995 of $u_{\max}$. Farther downstream, locations $y[(\rho u)_{\max}]$ and $y[u_{\max}]$ are equal. These changes from a single upper integration limit in the determination of δ^* and θ were made because they lead to a considerable improvement in the comparisons of the numerical and experimental results in the regions of significant pressure gradient normal to the flow direction. The effect of numerous choices of the upper integration limit was evaluated numerically before the one used to obtain the results of Figs. 9 and 10 was selected.[21] With this choice of the upper limit of integration, the numerical results show good overall agreement with the measurements although the increase in δ^* with increasing Mach number was not quite as large as observed in the experiments. This difference can be attributed to the differences between the measured and computed velocity profiles noted earlier.

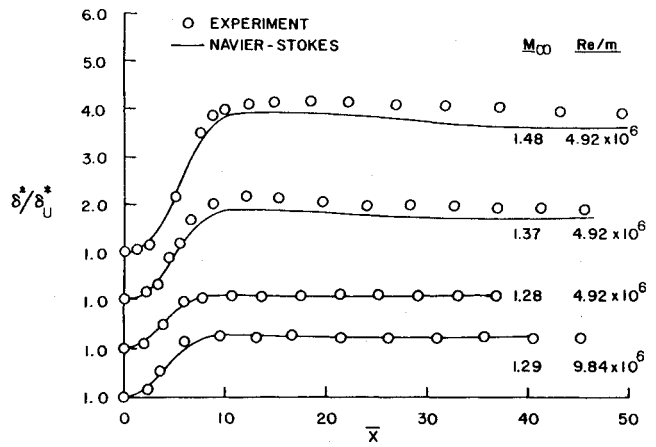

Fig. 9 Displacement thickness distribution.

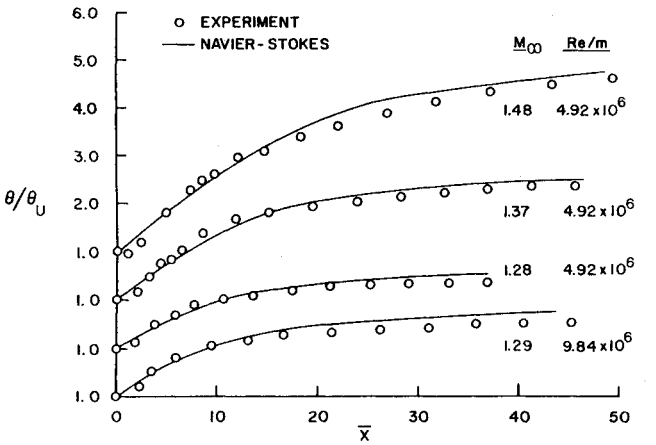

Fig. 10 Momentum thickness distribution.

Two-Dimensionality of the Flow

A limited investigation of the two-dimensionality of the flowfield was carried out. Wall pressure measurements with pressure taps located at 90-deg intervals around the periphery of the test section upstream of, within, and downstream of the interaction, differed by less than 0.5% at any particular axial location. Boundary-layer velocity profiles measured at 90-deg intervals around the circumference at the start of interaction and just downstream of the reattachment point show good agreement.[21] Finally, an indirect check of the two-dimensionality was performed by substituting measured integral properties ($C_f = 0$ was used for the separated region using the separation point indicated by the alcohol technique) and wall pressure into the momentum balance:

$$\frac{\rho_e u_e^2\left(\theta-\frac{\theta^2}{2R}\right)}{\left[\rho_e u_e^2\left(\theta-\frac{\theta^2}{2R}\right)\right]_u}-1=\int_{x_u}^{x}\frac{\left(\delta^*-\frac{\delta^{*2}}{2R}\right)\frac{dP}{dx}\,dx}{\left[\rho_e u_e^2\left(\theta-\frac{\theta^2}{2R}\right)\right]_u}$$

$$+\int_{x_u}^{x}\frac{\frac{C_f}{2}\,\rho_e u_e^2 dx}{\left[\rho_e u_e^2\left(\theta-\frac{\theta^2}{2R}\right)\right]_u}$$

The momentum thickness obtained from the right-hand side of the equation is compared with the experimental momentum thickness. The experimental momentum thickness was found to rise more rapidly than the calculated value. For the freestream Mach number of 1.28, a maximum difference of 2.25% was found just downstream of the shock wave. For the freestream Mach number of 1.48, a maximum difference of 11.8% was found near the reattachment point. The difference reduced to 5.2% at $\bar{X} = 48.99$. These differences may arise due to errors in the measurement of velocity profiles in the separation region, as discussed earlier. These observations are no absolute proof of two-dimensionality, but they suggest that the three-dimensional effects, if any, are very small.

Conclusions

The results of the present experimental investigation of a normal shock-wave/turbulent boundary-layer interaction in a circular duct have led to the following conclusions:

At the Reynolds numbers examined in the present study, a blockage of about 2.25% reduces the extent of separation in comparison with planar two-dimensional experiments with lower blockage. The shape of the embedded supersonic region is found to be very different from that observed in planar two-dimensional experiments. With increasing Mach number, the slope of the initial pressure rise increases, the flow becomes increasingly separated, and the embedded supersonic region gets larger. For the range of Reynolds number variation which could be achieved in the present study, the Reynolds number effect on an unseparated interaction is small.

Numerical simulations incorporating the Wilcox-Rubesin, two-equation turbulence model predicted the above experimental observations very well. This numerical study confirmed that with this turbulence model details of a relatively complex normal shock-wave/turbulent boundary-layer interaction flow could be reliably predicted. This is especially true when the flow does not separate. The simulation is not as accurate when the flow separates and becomes even less so if the separation becomes large. For the present study, this inaccuracy manifests itself by the inability of the simulation to predict precisely the skin friction, or velocity profiles adjacent to the wall within the separated region and downstream of reattachment where the experimental velocities recover to the undisturbed state more slowly than the calculated velocities.

Acknowledgments

The experimental work in this study was supported by NASA Grants NGR-48-002-047 and NGR-48-002-041 under the administration of Aerodynamics Branch, Ames Research Center.

References

[1]Mateer, G. G. and Viegas, J. R., "Effect of Mach and Reynolds Numbers on a Normal Shock-Wave/Turbulent Boundary-Layer Interaction," AIAA Paper 79-1502, July 1979.

[2]Seddon, J., "The Flow Produced by Interaction of a Turbulent Boundary Layer with a Normal Shock Wave of Strength Sufficient to Cause Separation," ARC R&M 3502, March 1960.

[3]Ackeret, J., Feldmann, F., and Rott, N., "Investigation of Compression Shocks and Boundary Layers in Gases Moving at High Speed," NACA TM 1113, Jan. 1947.

[4]Gadd, G. E., "Interactions Between Normal Shock Waves and Turbulent Boundary Layers," ARC R&M 3262, Feb. 1961.

[5]Vidal, R. J., Wittliff, C. E., Catlin, P. A., and Sheen, B. H., "Reynolds Number Effects on the Shock Wave—Turbulent Boundary-Layer Interaction at Transonic Speeds," AIAA Paper 73-661, July 1973.

[6]Kooi, J. W., "Influence of Free-Stream Mach Number on Transonic Shock Wave Boundary Layer Interaction," *Symposium on Transonic Configuration*, NLR-MP-78013-U, June 1978.

[7]East, L. F., "The Application of a Laser Anemometer to the Investigation of Shock-Wave Boundary Layer Interactions," *AGARD Conference on Applications of Non-Intrusive Instrumentation in Fluid Flow Research*, AGARD-CP-193, 1976.

[8]Mateer, G. G., Brosh, A., and Viegas, J. R., "A Normal Shock-Wave Turbulent Boundary-Layer Interaction at Transonic Speeds," AIAA Paper 76-161, July 1976.

[9]Green, J. E., "Interactions Between Shock Waves and Turbulent Boundary Layers," *Progress in Aeronautical Sciences*, Vol. 11, 1970, pp. 235-340.

[10]Reda, D. C. and Murphy, J. D., "Shock-Wave—Turbulent Boundary Layer Interactions in Rectangular Channels," AIAA Paper 72-715, 1972.

[11]Rose, W. C., "The Behavior of a Compressible Turbulent Boundary Layer in a Shock-Wave-Induced Adverse Pressure Gradient," NASA TN D-7092, March 1973.

[12]Gray, J. D., "Evaluation of Probes for Measuring Static Pressure in Supersonic and Hypersonic Flows," AEDC-TR-71-265, Jan. 1972.

[13]Om, D., "A Study of Transonic Normal Shock Wave/Turbulent Boundary Layer Interactions in Axisymmetric Internal Flow," Ph.D. Dissertation, University of Washington, Seattle, Wash., 1982.

[14]Reed, T. D., Pope, T. C., and Cooksey, J. M., "Calibration of Transonic and Supersonic Wind Tunnels," NASA CR 2920, Nov. 1977.

[15]Viegas, J. R. and Horstman, C. C., "Comparison of Multiequation Turbulence Models for Several Shock Separated Boundary Layer Interaction Flows," *AIAA Journal*, Vol. 17, Aug. 1979, pp. 811-820.

[16]Wilcox, P. C. and Rubesin, M. W., "Progress in Turbulence Modeling for Complex Flow Fields, Including the Effects of Compressibility," NASA TP 1517, 1980.

[17]*Proceedings 1980-1981 AFOSR-HTTM-Stanford Conference on Complex Turbulent Flows: Comparison of Computation and Experiment*, Stanford, Calif., Sept. 1981.

[18]MacCormack, R. W., "Numerical Solution of the Interaction of a Shock Wave with a Laminar Boundary Layer," *Lecture Notes in Physics*, Vol. 8, Springer-Verlag, 1971, pp. 151-163.

[19]MacCormack, R. W., "An Efficient Numerical Method for Solving the Time-Dependent Compressible Navier-Stokes Equations at High Reynolds Number," *Computing in Applied Mechanics*, AMD, Vol. 18, ASME, New York, 1976.

[20]Viegas, J. R. and Coakley, T. J., "Numerical Investigation of Turbulence Models for Shock Boundary-Layer Flows," *AIAA Journal*, Vol. 16, April 1978, pp. 293-294.

[21]Om, D., Viegas, J. R., and Childs, M. E., "An Experimental Investigation and a Numerical Prediction of a Transonic Normal Shock Wave/Turbulent Boundary Layer Interaction," AIAA Paper 82-0990, June 1982.

[22]Sun, C. C. and Childs, M. E., "A Modified Wall-Wake Velocity Profile for Turbulent Compressible Boundary Layers," *Journal of Aircraft*, Vol. 10, June 1973, pp. 381-383.

[23]Winter, K. G. and Gaudet, L., "Turbulent Boundary-Layer Studies at High Reynolds Numbers at Mach Numbers Between 0.2 and 2.8," ARC R&M 3712, 1970.

[24]Om, D. and Childs, M. E., "An Experimental Investigation of Multiple Shock Wave/Turbulent Boundary Layer Interactions in a Circular Duct," AIAA Paper 83-1744, July 1983.

[25]Rubesin, M. W., Murphy, J. D., and Rose, W. C., "Wall Shear in Strongly Retarded and Separated Compressible Turbulent Boundary Layers," *AIAA Journal*, Vol. 12, Oct. 1974, pp. 1442-1444.

[26]Padova, C., Falk, T. J., and Wittliff, C. E., "Experimental Investigation of Similitude Parameters Governing Transonic Shock-Boundary Layer Interactions," AIAA Paper 80-0158, Jan. 1980.

[27]Mathews, D. C., Childs, M. E., and Paynter, G. C., "Use of Coles' Universal Wake Functions for Compressible Turbulent Boundary Layers," *Journal of Aircraft*, Vol. 7, March-April 1970, pp. 137-140.